Environ. Sci. Technol. **2007**, *41,* 5846−5853

Mechanism of the Photocatalytic Degradation of C.I. Reactive Black 5 at pH 12.0 Using $SrTiO_3/CeO_2$ as the Catalyst

SHUANG SONG, LEJIN XU, ZHIQIAO HE,* AND JIANMENG CHEN

College of Biological and Environmental Engineering, Zhejiang University of Technology, Hangzhou 310032, People's Republic of China

XIUZHEN XIAO AND BING YAN*

Department of Chemistry, Tongji University, Shanghai 200092, People's Republic of China

The photocatalytic degradation mechanism of an azo dye, C.I. Reactive Black 5 (RB5), has been investigated in an aqueous suspension of $SrTiO_3/CeO_2$ composite under 250 W UV irradiation at pH 12.0. The process was studied by monitoring the change in RB5 concentration and the intermediate products employing UV−visible spectrophotometry, ion chromatography (IC), and gas chromatography/mass spectrometry (GC/MS) techniques and depletion in total organic carbon (TOC) content as a function of irradiation time. The adsorption peaks at wavelengths of 600, 312, and 254 nm were identified as the chromophore structure, and the naphthalene and benzene components of RB5, respectively. Little influence of iodide ion, *tert*-butyl alcohol, fluoride ion, or persulfate ion as h_{vb}^+, $^{\cdot}OH$, or e_{cb}^- scavengers on the decolorization proved that the decolorization of RB5 primarily proceeded by photolysis and/or $O_2^{\cdot-}$ in the bulk solution. After the decolorization, the process could shift progressively from the bulk solution to the surface of the catalysts and cleavage of the naphthalene and benzene rings was mainly attributed to the h_{vb}^+ pathway and $^{\cdot}OH_{ads}$ reactions, which was further verified by the effect of scavengers.

Introduction

Recently, a family of perovskite-type oxides with high performance in heterogeneous photocatalysis has been developed (*1*−*3*). Even though such kinds of oxide have been used in photocatalytic degradations of azo dyes (*4*), no further information about the role of the primary oxidative species or the photocatalytic mechanism has been provided. Generally, three different mechanisms are considered to explain the different performances among the heterogeneous photocatalysis processes (*5*). Stefan et al. (*6*) have suggested that the oxidation of methyl *tert*-butyl ether is initiated by free radicals (including $^{\cdot}OH$) in the solution, which are mainly induced by photogenerated hole−electron pairs. However, many researchers have stated that the organic compound has to be first adsorbed on the catalyst surface and then reacts with the photogenerated hole−electron pairs or surface-bound $^{\cdot}OH$ to form the final products (*7*−*9*). The third proposal involves both a surface reaction via holes/surface-bound $^{\cdot}OH$ and a solution reaction via free radicals (*10*).

When the photodegradation of an azo dye is conducted in the absence of a catalyst, the possible pathways in the presence of dissolved oxygen are homolysis of the excited dye into radicals, electron transfer of the excited dye to form a radical dye cation, decomposition by the superoxide radical anion ($O_2^{\cdot-}$), and decomposition by singlet oxygen (*11*). In the field of photocatalysis, there has been much debate as to whether photoreactions occurring on the surface involve reactions with positive holes (h_{vb}^+) or surface-bound $^{\cdot}OH$ or in solution with free radicals (*10*, *12*). In aerated systems, dioxygen acts as an efficient electron scavenger to trap the conduction band electron to yield superoxide radical anions, $O_2^{\cdot-}$ (*13*). Early studies reported that the initial photoreaction process appeared to vary according to the model pollutants and experimental conditions (*14*). Despite these studies, no major efforts have been made to study the detailed mechanisms of the photocatalytic oxidation processes by UV−visible absorption spectra of dye solutions.

Alkali rare earth titanates, such as $SrTiO_3$, belong to typical perovskite-type complex oxides, whose basic framework is a Ti−O polyhedron, just like TiO_2. Consequently, $SrTiO_3$ also presents a similar energy band structure, resulting in similar semiconductivity. Furthermore, $SrTiO_3$ shows a wide absorption band in the ultraviolet region in the range 300−400 nm (*15*). So it can be predicted that $SrTiO_3$ may produce a photocatalytic effect similar to that for some special reaction systems. CeO_2 can exhibit strong ultraviolet absorption in the range 300−450 nm (*16*), and its incorporation into $SrTiO_3$ can enhance ultraviolet absorption. Thus, it can be predicted that the composite fabricated $SrTiO_3/CeO_2$ may be a candidate for photocatalytic reaction of special pollutants.

In this study, we have chosen an azo dye, C. I. Reactive Black 5 (RB5), as a model contaminant for investigating the degradation mechanism and reaction pathways of photocatalytic oxidation using a $SrTiO_3/CeO_2$ composite as the catalyst at pH 12.0. The feasibility of the $SrTiO_3/CeO_2$ composite which belongs to the representative perovskite-type oxides was testified by the characterization of the catalyst. Investigating characteristic absorption bands of RB5 at 254, 312, and 600 nm, the detailed mechanism of the photocatalytic oxidation of RB5 at pH 12.0 was elucidated through the use of different h_{vb}^+, $^{\cdot}OH$, and e_{cb}^- scavengers and verified by total organic carbon (TOC) analysis, UV−visible spectroscopy, ion chromatography (IC), and gas chromatography/mass spectrometry (GC/MS) techniques.

Experimental Section

Materials and Reagents. All major chemicals were of reagent grade or higher. C.I. Reactive Black 5 was supplied by Zhejiang Runtu Co., Ltd., China. Strontium carbonate, ceria (cerium oxide, CeO_2), and tetrabutyl titanate for preparation of the $SrTiO_3/CeO_2$ catalyst were obtained from Shanghai, China. Potassium iodide (KI), sodium fluoride (NaF), potassium persulfate ($K_2S_2O_8$), and *tert*-butyl alcohol (*t*-BuOH) used as scavengers were purchased from Zhejiang, China. Nitrogen was supplied by Zhejiang Dazhong Co., Ltd., China. Deionized and doubly distilled water was used throughout this study.

Preparation and Characterization of the Photocatalyst. The $SrTiO_3/CeO_2$ solid powder was synthesized by a dry (for $SrCO_3$ and CeO_2)−wet (sol−gel for $Ti(OC_4H_9)_4$) composition

* Address correspondence to either author. Phone: 86-571-88320726 (Z.H.), 86-21-65984663 (B.Y.). Fax 86-571-88320276 (Z.H.), 86-21-65982287 (B.Y.). E-mail: zqhe@zjut.edu.cn (Z.H.), byan@tongji.edu.cn (B.Y.).

10.1021/es070224i CCC: $37.00
Published on Web 07/10/2007

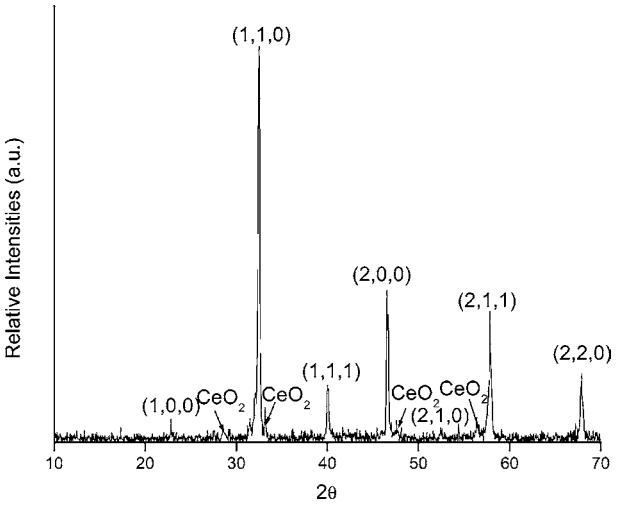

FIGURE 1. XRD pattern of $SrTiO_3/CeO_2$.

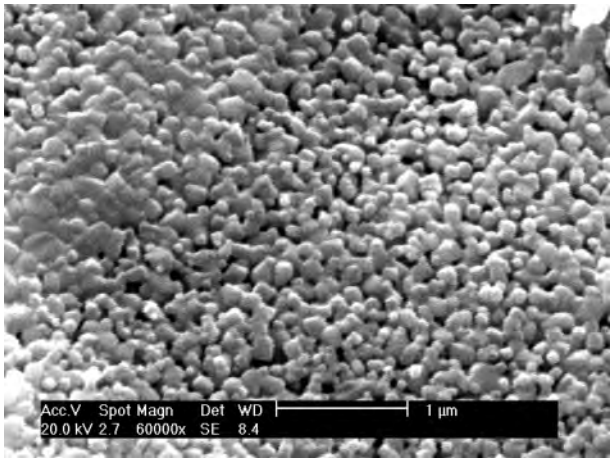

FIGURE 2. SEM micrographs of $SrTiO_3/CeO_2$.

method: concentrated nitric acid was added to the $SrCO_3$ starting material. Then the white powders were dissolved in double-distilled water. The solution was mixed with CeO_2 and stirred for an hour. At the same time, $Ti(OC_4H_9)_4$ was added to the solution and its pH value was adjusted to 7.0−8.0 with ammonia solution. After stirring for 1 h at 80 °C, the yellow gel precursors were formed. The gel precursors were calcined twice at different temperatures. First, the gel was heated at 600 °C for 5 h and then the powders were ground again. Finally, the product was obtained after 5 h at 1000 °C.

The particle size was determined by X-ray diffraction (XRD, Bruker, D8-Advance, 40 kV and 20 mA, Cu Kα) and scanning electronic microscopy (SEM, Philips XL-30). The solid-state ultraviolet−visible spectrum was measured with an Instant SpecTM-BWS003 spectrophotometer.

Photochemical Experiments. The dye solution was placed into a cylindrical Pyrex glass reactor (diameter 12 cm; height 15 cm; total capacity 1000 mL). At the reactor center, a mercury lamp of 250 W (Philips YPZ220) equipped with a quartz tube was located and immersed in the dye solution. The output of the mercury lamp peaks at 365 nm and is significant in the range 250−450 nm. The UV lamp was attached to a power supply (Philips HID, Beijing, China). Gases were purged through a small glass gas dispersion tube with coarse porosity placed at the bottom of the reaction cylinder to ensure small bubble formation for effective purging continuously throughout experiments. There was a port at the top of the reactor for measuring temperature and withdrawing samples. During the reaction, a water-cooling system cooled the water-jacketed photochemical reactor to

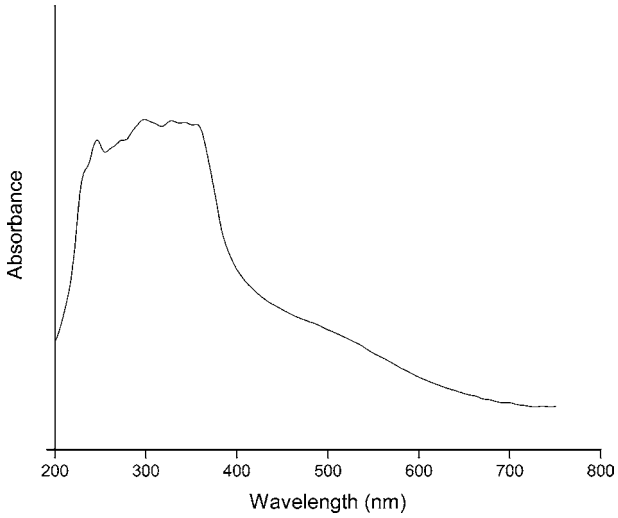

FIGURE 3. UV−visible absorption spectrum of $SrTiO_3/CeO_2$.

maintain the solution at 25(±1) °C. The operating conditions of the thermostat (THD-2015, Tianheng Instrument Factory, Ningbo, China) in the system were capacity 15 L, pump flow rate 6 L min^{-1}, and set temperature 8 °C.

Separate experimental results showed that, when catalyst concentrations of 0.01, 0.02, 0.03, 0.1, 0.5, 1.0, and 1.5 g L^{-1} were used, the best catalyst concentration was 0.02 g L^{-1}. Phosphate buffers were prepared previously in deionized water by mixture of calculated amounts of sodium hydroxide solution and phosphoric acid solution to yield an ionic strength of 0.0667 mol L^{-1}. A 100 mg L^{-1} dye solution was prepared by dissolving 100 mg of RB5 in 1000 mL of phosphate buffer. For the purging nitrogen gas experiments, pH adjustments were conducted before purging the system with the desired gases at a flow rate of 0.2 m^3 h^{-1} for 30 min to give the desired oxygen level prior to the experiments. For experiments with scavengers, the calculated amount of scavengers was added to the RB5 solution. Thereafter, 4−8 mL samples were withdrawn at predetermined time intervals. These samples were centrifuged and filtered through a 0.45 μm membrane filter to remove the catalyst particles before analysis.

Sample Analysis. A UV−visible spectrophotometer (T6, Beijing Purkinje General Instrument Co., Ltd.) was used for the determination of UV absorbance in the range 200−900 nm. The solution pH was measured with a pHs-25 instrument (Rex Analytical Instrument Co. Ltd., Shanghai, China). To determine the extent of mineralization of RB5 in solution under different conditions, the total organic carbon of the reaction solution was measured with a TOC−V_{CPH} total organic carbon analyzer.

Sulfate (SO_4^{2-}) was determined using an ion chromatograph. A Dionex model ICS 2000 ion chromatograph equipped with a dual-piston (in series) pump, a Dionex IonPac AS19 analytical column (4 mm × 250 mm), and an IonPac AG19 guard column (4 mm × 250 mm) were used throughout. The detection was performed with a Dionex DS6 conductivity detector. Suppression of the eluent was achieved with a Dionex anion ASRS electrolytic suppressor (4 mm) in the autosuppression external water mode.

To identify the intermediate products of RB5 photocatalytic degradation, a Varian cp3800 gas chromatograph and a Varian Saturn 2000 mass spectrometer were used. A WCOT fused silica series column (30 m × 0.25 mm, 0.25 μm film thicknesses) was employed and the temperature was programmed at 80 °C for 1 min, then ramped up to 250 °C at a rate of 12 °C min^{-1}, and held at 250 °C for 5 min. The other experimental conditions were EI impact ionization 70 eV,

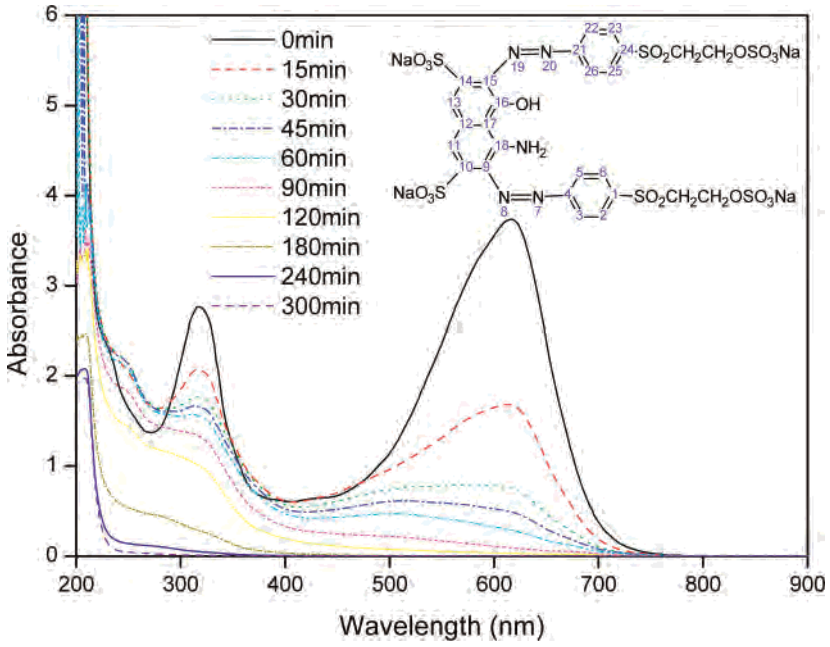

FIGURE 4. UV−visible absorption spectral changes of the RB5 (100 mg L^{-1}) solution in $SrTiO_3/CeO_2$ (0.02 g) dispersion at pH 12.0 under 250 W UV irradiation.

TABLE 1. Intermediates Identified by GC/MS and IC

pH	Symbol	Compounds	Structural formula	Analytical methods		Sample time (min)				
				GC/MS	IC	45	120	210	300	420
4.0	D_1	5,8-dioxo-3,4-didehydro-5,8-dihydronaphthalene-1-sulfonic acid		√		√	√	√	√	√
4.0	D_2	phenol		√		√	√	√	√	√
4.0	D_3	(2Z)-but-2-enedioic acid		√		√	√	√	√	√
4.0	D_4	oxalic acid	$(COOH)_2$	√		√	√	√	√	√
4.0	D_5	sulfate	SO_4^{2-}		√					
12.0	D_1	5,8-dioxo-3,4-didehydro-5,8-dihydronaphthalene-1-sulfonic acid		√		√	√			
12.0	D_2	phenol		√		√	√	√		
12.0	D_3	(2Z)-but-2-enedioic acid		√		√	√	√	√	√
12.0	D_4	oxalic acid	$(COOH)_2$	√		√	√	√	√	√
12.0	D_5	sulfate	SO_4^{2-}		√			√	√	√

helium as the carrier gas, injection temperature 280 °C, and source temperature 100 °C.

Results and Discussion

Catalyst Characterization. The representative XRD pattern (Figure 1) shows that the $SrTiO_3/CeO_2$ product was predominantly crystallized in the cubic system with space group $Pm\bar{3}m$ for high thermolysis temperature, in agreement with JCPDS (86-0179). While some additional weak peaks could also be observed, indicating that there exists some CeO_2 phase and the Ce^{4+} cannot substitute Ti^{4+} completely. In addition, we obtained values of about 21−67 nm for the particle diameter.

Scanning electron microscope (SEM) images for $SrTiO_3/CeO_2$ solids shows the homogeneous microstructure and micromorphology (Figure 2). There are some conglomeration phenomena in the SEM micrograph for the high temperature of thermal decomposition. It can be predicted that $SrTiO_3/CeO_2$ particle size was in the range 50−100 nm.

The photoabsorption property (UV−visible absorption spectrum) for $SrTiO_3/CeO_2$ composite catalyst (Figure 3) shows that the broad absorption bands from 200 to 700 nm especially the strong absorption in the ultraviolet region (200−400 nm) suggest the effective photoabsorption property for this oxide composite photocatalyst system. Besides, the absorption in ultraviolet region may be mainly ascribed to the absorption of titanate host framework while not CeO_2 (central absorption peak should situate at 400 nm), revealing that the main absorption is due to the solid solution system of $SrTiO_3/CeO_2$.

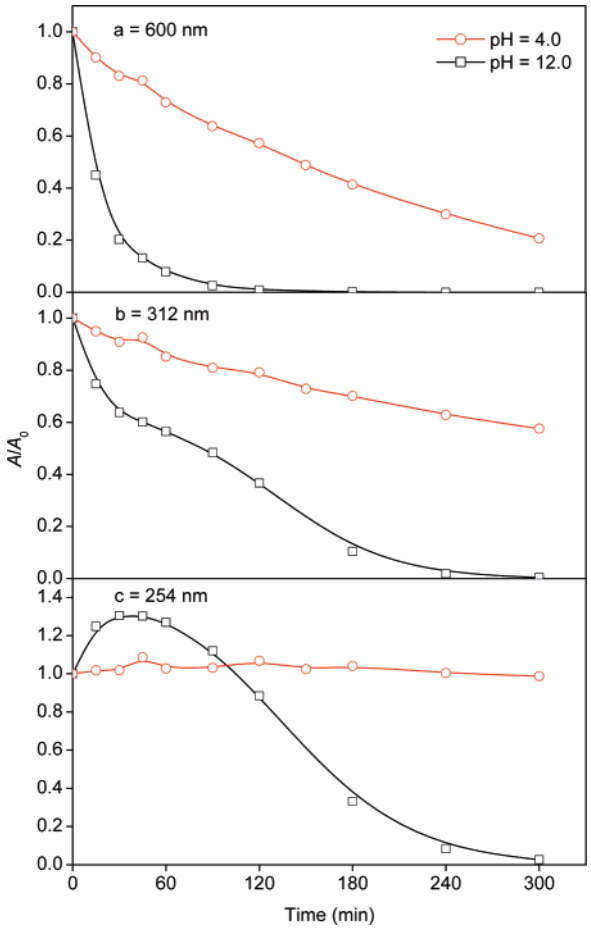

FIGURE 5. Effect of pH (4.0 and 12.0) on the photodegradation of 100 mg L^{-1} RB5 determined by the abatements at UV-600 (a), UV-312 (b), and UV-254 nm (c) bands with 0.02 g of catalyst and 250 W UV.

Identification of the Absorption Peaks. As shown in Figure 4, the spectrum of RB5 before photodegradation generally exhibits three main peaks at wavelengths of 600, 312, and 254 nm. The absorption spectra shown in Figure 4 reveal no new intermediates or products formed that would have manifested new absorption features in the visible and ultraviolet region. The characteristic absorption peak at 600 nm in the visible band, used to measure the decolorization of the dye solution, can be attributed to a chromophore containing a long conjugated π-system linked by two azo groups (*17*). The absorption peaks at 312 and 254 nm conform theoretically to the naphthalene and benzene components, respectively, in the molecular structure (*18*, *19*), which are assigned to the $\pi-\pi^*$ transition of the electrons in the π bonding orbital to the π^* antibonding orbital of the double bond system. During the experimental process, soluble acid, base, and salt formed may disturb the absorbance of UV−visible spectroscopy. However, combined with the intermediates detected at retention times of 300 and 420 min (Table 1) and the UV−visible spectra after a reaction time of 300 min (Figure 4), the compounds without naphthalene and benzene groups formed in the reaction had little influence on the identification of the absorption peaks.

The pH of the solution significantly affects the degradation of RB5 (*20*). A separate experiment showed that the poorest degradation result was obtained at pH 4.0 and the best was obtained at pH 12.0. Hence, experiments were conducted at the two initial pH values to investigate the effect of pH on the degradation of RB5 (Figure 5). Quantification was performed by measuring the UV absorbance at 600, 312, and 254 nm. Figure 5a shows that complete dye decolorization was almost achieved at the two pH values and the decolorization rate at pH 12.0 was noticeably faster. From Figure 5b it is evident from the UV 312 nm absorption band that the degradation rate at pH 4.0 proceeded considerably slower compared to the degradation rate at pH 12.0. Figure 5c delineates that in the UV 254 nm absorption band there was no significant photocatalytic oxidation of RB5 at pH 4.0. The initial curve increase at pH 12.0 may be due to the formation of benzene rings by fragmentation of the naphthalene component, which then decreases gradually (*18*). The majority of the experiments reported in this paper were carried out at pH 12.0.

Further convincing evidence to explain the trend described in Figure 5 was obtained by a comparison of the TOC removal at pHs 4.0 and 12.0 and measurement of the intermediates generated during the photodegradation of RB5 at pHs 4.0 and 12.0. Note that 57% of the TOC was removed after a reaction time of 300 min at pH 12.0, whereas only 10% TOC removal was observed at pH 4.0 (Figure 6). The result clearly suggests that lower mineralization of RB5 was achieved at pH 4.0, indicating that more carbonaceous substances existed in the solution, in accordance with the concentration of RB5 examined by UV−visible spectroscopy and the intermediates identified by GC/MS analysis. As shown in Table 1, compound D_1 was not detected at retention times of 210, 300, and 420 min at pH 12.0, whereas D_1 always existed during the reaction at pH 4.0, which was consistent with loss of sulfate ions from the D_1 molecule analyzed by IC. Figure 5b also shows that, after 210 min of irradiation, nearly all of the naphthalene component was decomposed at pH 12.0 but only partial degradation of the naphthalene component took place at pH 4.0. On the basis of all the analyses discussed above, the absorption maximum at 254 nm mainly corresponds to phenol (D_2) in the RB5 structure.

Generally, the typical wavelength of naphthalene and condensed ring aromatics is above 300 nm, and the benzene group has a high absorbance at about 254 nm. Hence, although there might be mutual interference between naphthalene and the benzene group in the intensity and wavelength of the absorbance peaks, this interference had little influence on the investigation of the overall tendency for ring cleavage in our experiments.

Decolorization of RB5. A comparison of the photolyses at pH 12.0 in the N_2-purged condition, air equilibrium condition (i.e., no gas purging), and O_2-purged condition was undertaken to obtain the decolorization mechanism of RB5. The reactor was open to the ambient air or purged with gases and stirred magnetically during the irradiation. The top of the reactor was not sealed and had a dissolved oxygen level of 0.3 mM; purging with N_2 continuously during the process reduced and maintained the O_2 levels to 0.005−0.02 mM. A separate experiment (data not shown) showed that additional O_2 purging did not result in a further increase in the decolorization rate. As seen in Figure 7a, one notable result is that the decolorization rate in the air equilibrium condition is clearly higher than that in the N_2 condition. In the N_2-purged condition, dissolved oxygen may not be sufficient to totally decolorize the dye whereas curve 1 shows that complete decolorization was achieved, indicating the importance of photolysis in the decolorization of RB5. Under an N_2 atmosphere, the decolorization rate of RB5 with 0.02 g of catalyst (curve 3) was higher than that without catalyst (curve 1), suggesting that in the anoxic condition the $SrTiO_3$/CeO_2 catalyst has an enhancing effect on the decolorization of RB5. However, in the air equilibrium condition, the decolorization of RB5 with 0.02 g of catalyst (curve 4) exhibited almost the same rate as that in the system without any catalyst (curve 2), which showed that the $SrTiO_3/CeO_2$ catalyst played a minor role in the decolorization of RB5. The data above illustrated that photolysis is important in the decolorization

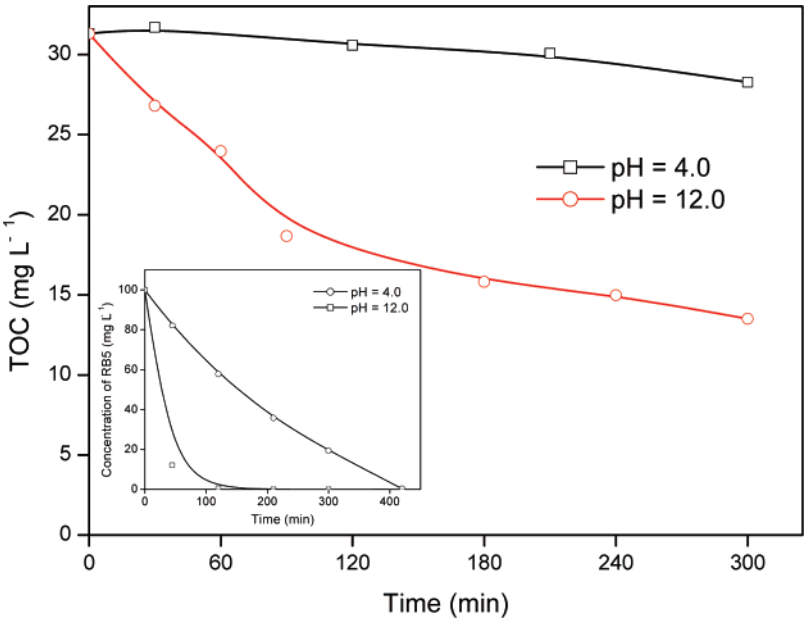

FIGURE 6. Comparison of the TOC removal at pH 4.0 and 12.0, where the dye concentration is 100 mg L^{-1} and the catalyst dose is 0.02 g under 250 W UV irradiation.

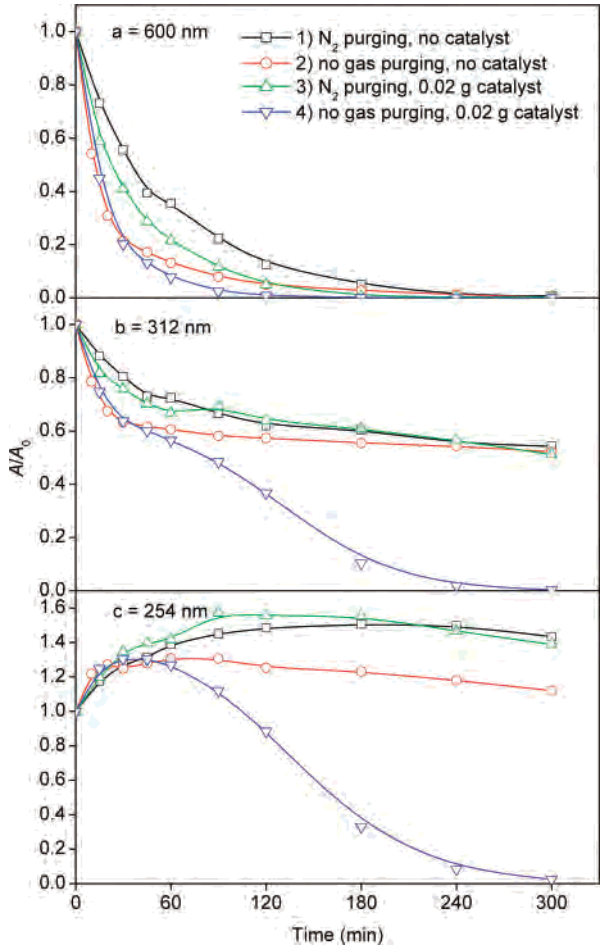

FIGURE 7. Photodegradation of 100 mg L^{-1} RB5 at UV-600 (a), UV-312 (b), and UV-254 nm (c) bands with pH 12.0 and 250 W UV under different conditions: N_2 purging without catalyst (curve 1); no gas purging without catalyst (curve 2); N_2 purging with 0.02 g of catalyst (curve 3); and no gas purging with 0.02 g of catalyst (curve 4).

of RB5 and air-equilibrated dissolved oxygen was sufficient for decolorization.

As seen in eq 1, the dye (D) and the excited dye (D*) can be decomposed by homolytic cleavage into radicals (X· and Y·). Oxygen can act as a photogenerated electron scavenger to give $O_2^{\cdot-}$ for the decolorization of RB5 in the absence of a photocatalyst by the mechanism shown in eqs 2−6 (*11*).

$$D + h\nu \rightarrow D^* \rightarrow X^{\cdot} + Y^{\cdot} \quad (1)$$

$$X^{\cdot} + O_2 \rightarrow XOO^{\cdot} \rightarrow X^+ + O_2^{\cdot-} \quad (2)$$

$$Y^{\cdot} + O_2 \rightarrow YOO^{\cdot} \rightarrow Y^+ + O_2^{\cdot-} \quad (3)$$

$$D^* + O_2 \rightarrow D^{\cdot+} + O_2^{\cdot-} \quad (4)$$

$$D + O_2^{\cdot-} \rightarrow \text{products} \quad (5)$$

$$D^{\cdot+} + H_2O \rightarrow \text{products} + OH^- \quad (6)$$

In the air equilibrium condition, the reason for the similar decolorization rate in the absence and presence of the catalyst could be attributed to the fact that the reactions shown in eqs 1−6 play an important role in decolorization. Superoxide radical anions ($O_2^{\cdot-}$) and hydroxyl radicals (·OH) generated at the surface of the catalysts are minor oxidants for the decolorization of RB5. If it is believed that the decolorization of RB5 mainly occurs in the bulk solution and not at the surface of the catalysts, then the reactive species generated on the surface of the $SrTiO_3/CeO_2$ catalyst would not be important factors that affect the decolorization rate. These results might be demonstrated by the addition of iodide, *t*-BuOH, fluoride, or persulfate as scavengers, which are discussed in a later section.

It should be noted that high temperature on the wall of the quartz tube might promote thermal decomposition of RB5. However, a dark control showed no significant decolorization after 300 min reaction indicating that thermal decomposition was negligible. The observations of these investigations clearly demonstrate the importance of photolysis and oxygen to the decolorization of RB5, which takes place in the bulk solution.

Ring Cleavage of the RB5 Molecule. The decline in the absorbance at 600 nm (see Figure 7a) may be attributed to decolorization of RB5 but not to full degradation. In order to investigate the degradation mechanism of RB5, cleavage of the naphthalene and benzene rings in the N_2-purged condition and air equilibrium condition was studied, as shown in Figures 7b and 7c. In the absence of the $SrTiO_3/CeO_2$ catalyst, little cleavage of the naphthalene or benzene rings was observed after complete dye decolorization in the N_2-purged condition (curve 1) or air equilibrium condition (curve 2). In the presence of 0.02 g of catalyst, cleavage of the naphthalene and benzene rings occurred only to a slight extent in the N_2-purged condition (curve 3), whereas the rings were cleaved completely in the air equilibrium condition (curve 4). We infer from the above data that both sufficient oxygen and $SrTiO_3/CeO_2$ semiconductor particles are indispensable for ring cleavage of the RB5 molecule.

The mechanism of photocatalysis in the presence of oxygen, summarized in eqs 7−17, has been proposed earlier (*14*, *21*−23). We deduce that cleavage of the naphthalene and benzene rings would be initiated by the attack of $\cdot OH_{ads}$, $\cdot OH_{free}$, and $O_2^{\cdot -}$ generated both in the bulk solution (eqs 2−4) and at the surface of the catalyst. The deduction will be manifested by the addition of scavengers, which are further discussed in the later part of this paper.

$$\text{photocatalyst} + h\nu \rightarrow h_{vb}^{+} + e_{cb}^{-} \quad (7)$$

$$h_{vb}^{+} + e_{cb}^{-} \rightarrow \text{heat} \quad (8)$$

$$h_{vb}^{+} + OH_{ads}^{-} \rightarrow \cdot OH_{ads} \quad (9)$$

$$h_{vb}^{+} + H_2O \rightarrow H_2O^{+} \rightarrow H^{+} + \cdot OH_{free} \quad (10)$$

$$e_{cb}^{-} + O_{2(ads)} \rightarrow O_2^{\cdot -} \quad (11)$$

$$O_2^{\cdot -} + e_{cb}^{-} (+ 2H^{+}) \rightarrow H_2O_2 \quad (12)$$

$$H_2O_2 + O_2^{\cdot -} \rightarrow \cdot OH_{ads} + OH^{-} + O_2 \quad (13)$$

$$H_2O_2 + e_{cb}^{-} \rightarrow \cdot OH_{ads} + OH^{-} \quad (14)$$

$$OH^{-} + h_{vb}^{+} \rightarrow \cdot OH_{ads} \quad (15)$$

$$\cdot OH/O_2^{\cdot -} + \text{dye} \rightarrow \text{degraded products} \quad (16)$$

$$h_{vb}^{+}/e_{cb}^{-} + \text{dye} \rightarrow \text{degraded products} \quad (17)$$

Verification of the Proposed Mechanism using Scavengers. The proposed mechanism was further verified by determining the influence of different scavengers on the degradation of RB5, as shown in Figure 8.

Effect of Iodide Ion. Iodide ion is a scavenger and reacts with h_{vb}^{+} and $\cdot OH_{ads}$ (*5*, *9*, *24*), reducing the number of oxidizing species available at the surface of the catalyst for reaction with RB5. The valence band hole is easily captured by I^{-} (the redox potential of the couple $I^{\cdot}/I^{-}$ is 1.3 V) and pathways due to oxidation by surface hydroxyl radicals are also possible because the rate constant of reaction with $\cdot OH_{ads}$ is 1.2×10^{10} M^{-1} s^{-1} (*25*).

When 20 mM KI was used as a diagnostic tool for suppressing the hole process and reducing $\cdot OH_{ads}$, the decolorization rate of RB5 was not decreased (Figure 8a). Accordingly, if the hole process and $\cdot OH_{ads}$ are effective for decolorization of RB5, the decolorization rate should be greatly decreased by addition of scavenger KI, which is inconsistent with the result shown in Figure 8a. The result supports the view that the decolorization mostly takes place in the bulk solution.

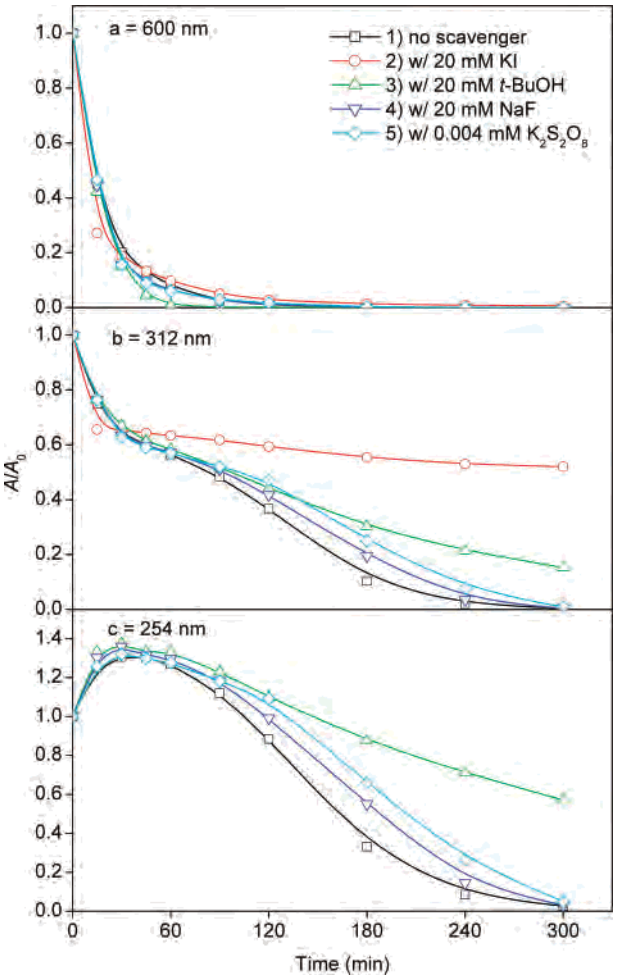

FIGURE 8. Effects of scavengers on the photodegradation of 100 mg L^{-1} RB5 at UV-600 (a), UV-312 (b), and UV-254 nm (c) bands with 0.02 g of catalyst and 250 W UV at pH 12.0: no scavenger (curve 1); 20 mM KI (curve 2); 20 mM *t*-BuOH (curve 3); 20 mM NaF (curve 4); and 0.004 mM $K_2S_2O_8$ (curve 5).

Cleavage of the naphthalene rings was strongly inhibited by the addition of excess KI, as shown in Figure 8b. This result suggests that the naphthalene rings were mainly cleaved by direct interaction with h_{vb}^{+} and/or by reaction with $\cdot OH_{ads}$. It should be noted that the effect of 20 mM KI on the determination wavelength for RB5 (254 nm) was huge because the absorption peak of KI is at the wavelength of 220 nm, so the effect of KI on the cleavage of benzene rings was not taken into account.

Effect of Tert-Butyl Alcohol. Excess *t*-BuOH (20 mM) was added to the solution to scavenger all the hydroxyl radicals produced in the system (*26*, *27*). *t*-BuOH can react quickly with $\cdot OH$ with a rate constant of 6.0×10^8 M^{-1} s^{-1} (*28*). As shown in Figure 8a, adding excess *t*-BuOH did not change the decolorization rate of RB5. This implies that hydroxyl radicals do not play a major role in the decolorization, although previous work (*26*) assumed that they were the main oxidant of RB5 decolorization in the UV/IO_4^{-} process, which further supported the conclusion that the decolorization of RB5 occurred in the bulk solution by photolysis and/or $O_2^{\cdot -}$ rather than by $\cdot OH$.

Cleavage of the naphthalene and benzene rings was moderately inhibited by excess *t*-BuOH (see Figure 8b and c). These phenomena clearly indicate that $\cdot OH$ was one of

the main oxidants responsible for the ring cleavage of RB5. Since the diffusion of surface-bound ·OH from the surface of the catalyst into the bulk solution is minimal (*7*), $\cdot OH_{ads}$ is the major oxidant among the hydroxyl radicals scavenged by *t*-BuOH. Combined with the results obtained by the effect of iodide ion, it can be concluded that the cleavage of the rings is dominated by the h_{vb}^+ pathway and $\cdot OH_{ads}$ reactions.

Effect of Fluoride. Since the redox potential of the couple $F^{\cdot}/F^-$ is about 3.6 V, F^- is very stable against oxidation even by h_{vb}^+ (*29*). Furthermore, the concentration of surface hydroxyl groups on the catalysts can be controlled by adopting fluoride exchange (*14*). Comparison of curves 1 and 4 (Figure 8a) shows that $\cdot OH_{ads}$ should not be responsible for RB5 decolorization since the addition of excess NaF (20 mM) did not reduce the decolorization rate of RB5.

As shown in Figure 8b and c, cleavage of the naphthalene and benzene rings was inhibited but occurred at a somewhat slower rate since the formation of $\cdot OH_{ads}$ was significantly inhibited and the replacement of the hydroxyl groups on the surface of the catalyst by fluoride ion increased h_{vb}^+ availability. It was deduced that the ring cleavage may be partially attributed to the $\cdot OH_{ads}$ mechanism, which provides further support for the ring cleavage mechanism.

Effect of Persulfate. The use of inorganic compounds such as $S_2O_8^{2-}$ has been demonstrated to trap the photogenerated electrons (*30*, *31*), as shown in eqs 18 and 19. The sulfate radical anion ($SO_4^{\cdot -}$) may react with a water molecule, producing ·OH (eq 20).

$$S_2O_8^{2-} + e_{cb}^- \rightarrow SO_4^{\cdot -} + SO_4^{2-} \quad (18)$$

$$SO_4^{\cdot -} + e_{cb}^- \rightarrow SO_4^{2-} \quad (19)$$

$$SO_4^{\cdot -} + H_2O \rightarrow \cdot OH + SO_4^{2-} + H^+ \quad (20)$$

As shown in Figure 8a, 0.004 mM $K_2S_2O_8$ showed a negligible effect on the decolorization of RB5, which suggests that $O_2^{\cdot -}$ generated at the surface of the catalyst (eq 11) and ·OH produced as in eq 20 are not the main oxidants in the decolorization of RB5.

Cleavage of the naphthalene and benzene rings was reduced in the presence of $K_2S_2O_8$, suggesting that the ring cleavage was inhibited (Figure 8b and c) due to the increase in concentration of SO_4^{2-} (*32*). The excess of SO_4^{2-} will be adsorbed on the surface of the catalyst, reducing the catalytic activity, and then the adsorbed SO_4^{2-} reacts with h_{vb}^+ and ·OH (eqs 21 and 22). Since $SO_4^{\cdot -}$ is less reactive than h_{vb}^+ and ·OH the excess SO_4^{2-} reduces the ring cleavage. Thus, the e_{cb}^- mechanism, as well as h_{vb}^+ and ·OH, is effective for the ring cleavage. In addition, it should be noted that the effect of 0.004 mM $K_2S_2O_8$ on the determination wavelength for RB5 (254 nm) was very little, so it was not taken into account.

$$SO_4^{2-} + h_{vb}^+ \rightarrow SO_4^{\cdot -} \quad (21)$$

$$SO_4^{2-} + \cdot OH \rightarrow SO_4^{\cdot -} + OH^- \quad (22)$$

In summary, RB5 molecules were first decolorized in the bulk solution, mostly initiated by photolysis and/or $O_2^{\cdot -}$. Then the process could shift from a decolorization reaction in the bulk solution to a surface reaction, cleaving the naphthalene and benzene rings. According to the effect of the scavengers, the ring cleavage was attributed to the action of h_{vb}^+, e_{cb}^-, and all the radicals, among which the h_{vb}^+ pathway and $\cdot OH_{ads}$ reactions play a dominant role. More research is required to determine whether the volatile organic compounds will influence the analyses of related parameters.

Possible Degradation Pathway of RB5. We propose the possible mechanistic steps in the photocatalytic degradation of RB5 at pH 12.0. The structure of RB5 is seen in Figure 4 and the intermediate compounds analyzed by GC/MS are shown in Table 1. The preferred sites of attack on RB5 by photolysis and/or $O_2^{\cdot -}$ were the 1, 4, 9, 15, 21, and 24 positions. The bonds C(4)−N(7), C(9)−N(8), C(15)−N(19), and C(21)−N(20) were probably cleaved and led to the decolorization of RB5 in the bulk solution. The intermediates formed by cleavage of bonds C(9)−N(8) and C(15)−N(19) were adsorbed on the surface of the catalysts and then rearranged. Afterward, naphthalene derivatives such as compound D_1 were generated primarily by the h_{vb}^+ mechanism and $\cdot OH_{ads}$ reactions. After the cleavage of C(4)−N(7) and C(21)−N(20) bonds, the fragments were adsorbed on the surface of the catalysts generating the benzene derivatives such as compound D_2 primarily by the h_{vb}^+ mechanism and $\cdot OH_{ads}$ reactions. Combined with the results of GC/MS analysis and UV−visible absorption spectra of RB5, the naphthalene derivatives such as compound D_1 could be further cleaved to form benzene derivatives (such as D_2) primarily by the h_{vb}^+ mechanism. Certainly, the naphthalene derivatives such as compound D_1 could be directly oxidized to smaller molecular organic acids such as D_3 and D_4, and the benzene derivatives such as compound D_2 were degraded to smaller molecular organic acids such as D_3 and D_4 with further reaction. Furthermore, sulfate (D_5) was partially obtained from sulfonic groups on RB5 molecules mainly via two pathways, namely the substitution by hydroxyl groups and the reaction with h_{vb}^+.

Acknowledgments

We are grateful for the financial support provided by the National Natural Science Foundation of China (Grant 50408024).

Literature Cited

(1) Saupe, G. B.; Zhao, Y.; Bang, J.; Yesu, N. R.; Carballo, G. A.; Ordonez, R.; Bubphamala, T. Evaluation of a new porous titanium-niobium mixed oxide for photocatalytic water decontamination. *Microchem. J.* **2005**, *81* (1), 156−162.

(2) Kim, H. G.; Becker, O. S.; Jang, J. S.; Ji, S. M.; Borse, P. H.; Lee, J. S. A generic method of visible light sensitization for perovskite-related layered oxides: Substitution effect of lead. *J. Solid State Chem.* **2006**, *179* (4), 1214−1218.

(3) Otsuka-Yao-Matsuo, S.; Omata, T.; Yoshimura, M. Photocatalytic behavior of cerium titanates, $CeTiO_4$ and $CeTi_2O_6$ and their composite powders with $SrTiO_3$. *J. Alloys Compd.* **2004**, *376* (1−2), 262−267.

(4) Sun, Z. S.; Chen, Y. X.; Ke, Q.; Yang, Y.; Yuan, J. Photocatalytic degradation of a cationic azo dye by TiO_2/bentonite nanocomposite. *J. Photochem. Photobiol., A* **2002**, *149* (1−3), 169−174.

(5) Li, W.; Wang, Y. Z. Photodegradation mechanism of two dyes: The influence of adsorption behavior on the novel TiO_2 particles. *J. Environ. Sci.-China* **2004**, *16* (2), 328−331.

(6) Stefan, M. I.; Mack, J.; Bolton, J. R. Degradation pathways during the treatment of methyl *tert*-butyl ether by the UV/H_2O_2 process. *Environ. Sci. Technol.* **2000**, *34* (4), 650−658.

(7) El-Morsi, T. M.; Budakowski, W. R.; Abd-El-Aziz, A. S.; Friesen, K. J. Photocatalytic degradation of 1, 10-dichlorodecane in aqueous suspensions of TiO_2: A reaction of adsorbed chlorinated alkane with surface hydroxyl radicals. *Environ. Sci. Technol.* **2000**, *34* (6), 1018−1022.

(8) Carraway, E. R.; Hoffman, A. J.; Hoffmann, M. R. Photocatalytic oxidation of organic-acids on quantum-sized semiconductor colloids. *Environ. Sci. Technol.* **1994**, *28* (5), 786−793.

(9) Yoon, S. H.; Lee, J. H. Oxidation mechanism of As (III) in the UV/TiO_2 system: Evidence for a direct hole oxidation mechanism. *Environ. Sci. Technol.* **2005**, *39* (24), 9695−9701.

(10) Sun, Y. F.; Pignatello, J. J. Evidence for a surface dual hole-radical mechanism in the TiO_2 photocatalytic oxidation of 2,4-dichlorophenaxyacetic acid. *Environ. Sci. Technol.* **1995**, *29* (8), 2065−2072.

(11) Zhao, W. R.; Wu, Z. B.; Shi, H. X.; Wang, D. H. UV photodegradation of azo dye Diacryl red X-GRL. *J. Photochem. Photobiol., A* **2005**, *171* (2), 97−106.
(12) Yang, T. C. K.; Wang, S. F.; Tsai, S. H. Y.; Lin, S. Y. Intrinsic photocatalytic oxidation of the dye adsorbed on TiO_2 photocatalysts by diffuse reflectance infrared Fourier transform spectroscopy. *Appl. Catal., B* **2001**, *30* (3−4), 293−301.
(13) Chen, C. C.; Lei, P. X.; Ji, H. W.; Ma, W. H.; Zhao, J. C.; Hidaka, H.; Serpone, N. Photocatalysis by titanium dioxide and polyoxometalate/TiO_2 cocatalysts. Intermediates and mechanistic study. *Environ. Sci. Technol.* **2004**, *38* (1), 329−337.
(14) Chen, Y. X.; Yang, S. Y.; Wang, K.; Lou, L. P. Role of primary active species and TiO_2 surface characteristic in UV-illuminated photodegradation of Acid Orange 7. *J. Photochem. Photobiol., A* **2005**, *172* (1), 47−54.
(15) Yamamoto, H.; Okamoto, S.; Kobayashi, H. Luminescence of rare-earth ions in perovskite-type oxides: from basic research to applications. *J. Lumin.* **2002**, *100* (1−4), 325−332.
(16) Yan, B.; Zhao, W. G. Wet chemical synthesis of nanometer CeO_2 with strong ultraviolet absorption property by in situ assembly of hybrid precursors. *Mater. Sci. Eng., B* **2004**, *110* (1), 23−26.
(17) Lucas, M. S.; Peres, J. A. Decolorization of the azo dye Reactive Black 5 by Fenton and photo-Fenton oxidation. *Dyes Pigm.* **2006**, *71* (3), 236−244.
(18) Gültekin, I.; Ince, N. H. Degradation of aryl-azo-naphthol dyes by ultrasound, ozone and their combination: Effect of α-substituents. *Ultrason. Sonochem.* **2006**, *13* (3), 208−214.
(19) Xie, Y. B.; Li, X. Z. Interactive oxidation of photoelectrocatalysis and eletro-Fenton for azo dye degradation using TiO_2-Ti mesh and reticulated vitreous carbon electrodes. *Mater. Chem. Phys.* **2006**, *95* (1), 39−50.
(20) Reutergàrdh, L. B.; Iangphasuk, M. Photocatalytic decolourization of reactive azo dye: A comparison between TiO_2 and CdS photocatalysis. *Chemosphere* **1997**, *35* (3), 585−596.
(21) Habibi, M. H.; Hassanzadeh, A.; Mahdavi, S. The effect of operational parameters on the photocatalytic degradation of three textile azo dyes in aqueous TiO_2 suspensions. *J. Photochem. Photobiol., A* **2005**, *172* (1), 89−96.
(22) Horikoshi, S.; Saitou, A.; Hidaka, H.; Serpone, N. Environmental remediation by an integrated microwave/UV illumination method. V. Thermal and nonthermal effects of microwave radiation on the photocatalyst and on the photodegradation of rhodamine-B under UV/Vis radiation. *Environ. Sci. Technol.* **2003**, *37* (24), 5813−5822.
(23) Cho, M.; Chung, H.; Choie, W.; Yoone, J. Linear correlation between inactivation of *E. coli* and OH radical concentration in TiO_2 photocatalytic disinfection. *Water Res.* **2004**, *38* (4), 1069−1077.
(24) Li, G. T.; Qu, J. H.; Zhang, X. W.; Liu, H. J; Liu, H. N. Electrochemically assisted photocatalytic degradation of Orange II: Influence of initial pH values. *J. Mol. Catal., A* **2006**, *259* (1−2), 238−244.
(25) Martin, S. T.; Lee, A. T.; Hoffmann, M. R. Chemical mechanism of inorganic oxidants in the TiO_2/UV process: Increased rates of degradation of chlorinated hydrocarbons. *Environ. Sci. Technol.* **1995**, *29* (10), 2567−2573.
(26) Lee, C.; Yoon, J. Application of photoactivated periodate to the decolorization of reactive dye: Reaction parameters and mechanism. *J. Photochem. Photobiol., A* **2004**, *165* (1−3), 35−41.
(27) Ou, Y.; Lin, J. D.; Zou, H. M.; Liao, D. W. Effects of surface modification of TiO_2 with ascorbic acid on photocatalytic decolorization of an azo dye reactions and mechanisms. *J. Mol. Catal., A* **2005**, *241* (1−2), 59−64.
(28) Chia, L. H.; Tang, X. M.; Weavers, L. K. Kinetics and mechanism of photoactivated periodate reaction with 4-chlorophenol in acidic solution. *Environ. Sci. Technol.* **2004**, *38* (24), 6875−6880.
(29) Yang, S. Y.; Lou, L. P.; Wang, K.; Chen, Y. X. Shift of initial mechanism in TiO_2-assisted photocatalytic process. *Appl. Catal., A* **2006**, *301* (2), 152−157.
(30) Haque, M. M.; Muneer, M.; Bahnemann, D. W. Semiconductor-mediated photocatalyzed degradation of a herbicide derivative, chlorotoluron, in aqueous suspensions. *Environ. Sci. Technol.* **2006**, *40* (15), 4765−4770.
(31) Wang, Y. B.; Hong, C. S. Effect of hydrogen peroxide, periodate and persulfate on photocatalysis of 2-chlorobiphenyl in aqueous TiO_2 suspensions. *Water Res.* **1999**, *33* (9), 2031−2036.
(32) Muruganandham, M.; Swaminathan, M. Photocatalytic decolourisation and degradation of Reactive Orange 4 by TiO_2-UV process. *Dyes Pigm.* **2006**, *68* (2−3), 133−142.

Received for review January 29, 2007. Revised manuscript received May 31, 2007. Accepted June 4, 2007.

ES070224I